ИНСТИТУТ ЯДЕРНОЙ ФИЗИКИ СО АН СССР

V.N.Baier, V.M.Katkov
and V.M.Strakhovenko

NONDIPOLE RADIATION OF ELECTRONS AT PLANAR CHANNELING

PREPRINT 84-116

НОВОСИБИРСК

NONDIPOLE RADIATION OF ELECTRONS AT PLANAR CHANNELING

V.N.Baier, V.M.Katkov
and V.M.Strakhovenko

Institute of Nuclear Physics,
630090, Novosibirsk 90, USSR

A b s t r a c t

The nondipole radiation of electrons is considered for any shape of interplane potential. A concrete analysis and comparison with the radiation of positrons have been carried out for a potential of the 'inverse parabola' type. It is shown that for description of the radiation of particles with energy $\varepsilon \lesssim 10$ GeV in the region of a maximum of the spectral distribution it is possible to take into account a few first harmonics at motion only. This substantially simplifies the calculation, especially for the potentials of complex shape. The diagrams which illustrate the radiation spectrum as a function of the angular width and of the direction of beam incidence on a thin crystal, have been depicted. A detailed comparison of the results with the experimental data available has been made.

1. Introduction

The present paper is dealt with the nondipole radiation of electrons at planar channeling. If the transverse momentum of a radiating particle is $p_\perp \ll m$, then one can use the dipole approximation; but if $p_\perp \gtrsim m$, then the radiation becomes significantly nondipole. Making allowance for the fact that $p_\perp \sim \varepsilon \vartheta_c$ ($\varepsilon(m)$ is the energy (mass) of a particle, ϑ_c is the Lindhard angle: $\vartheta_c = \sqrt{2U_0/\varepsilon}$ and U_0 is the depth of a potential well), we have $p_\perp/m \sim \sqrt{\rho_0}$, where ρ_0 is the parameter introduced in /1/:

$$\rho_0 = \frac{2\varepsilon U_0}{m^2} \tag{1.1}$$

So, at $\rho_0 \gtrsim 1$ ($\varepsilon \gtrsim \varepsilon_{nd} = m^2/2U_0$) the radiation gets nondipole. For the (110) plane, $\varepsilon_{nd} \simeq 5.2$ GeV in $Si(d)$ ($U_0 = 25$ eV) and $\varepsilon_{nd} \simeq 0.93$ GeV in W ($U_0 = 140$ eV). The planar-channeling radiation in the nondipole region has been discussed in Refs. /1-6/.

The effect under study is, in fact, a manifestation of the general mechanism of radiation at quasiperiodic motion (periodic in the frame moving with the particle's average velocity). It is this mechanism which determines radiation in undulators and in the field of a monochromatic plane wave. A theory of radiation during quasiperiodic motion, including the quantum region where the radiation recoil should be taken into consideration, has been developed by the authors in /1,7/.

In application to the channeling radiation problem, the radiation characteristics, calculated in /1,7/, are to be averaged over the states with different transverse energy $\varepsilon_\perp$:

$$\varepsilon_\perp = \frac{p_\perp^2}{2\varepsilon} + U(x) \tag{1.2}$$

where $U(x)$ is the interplane potential, taking into account the dependence of the motion parameters on $\varepsilon_\perp$.

The motion of electrons in any adequate potential of the crystal planes is a non-harmonic one. This circumstance signi-

ficantly complicates the solution of the radiation problem in comparison with the case of positrons for which the oscillator potential can be employed in the nondipole region (this question has been discussed in /5/). The latter enables the analytical stage in calculations to be substantially advanced. The radiation from positrons in the nondipole region has been analysed in the authors' paper /5/ (see /4,6/ as well) which contains also a comparison with experiments. For electrons, a detailed consideration is made in the present paper.

2. Description of the radiation for arbitrary potential at a given transverse energy

With an arbitrary potential of the planar channeling, for the radiation spectrum at a given value of $\mathcal{E}_\perp$ we have

$$\frac{dI}{d\omega} = \frac{i\alpha\omega}{(2\pi\gamma)^2}\int_{-\infty}^{+\infty}\frac{dt}{t-i0}\int_{-\pi}^{\pi}d\tau\left[1+\frac{a(\omega)}{2}\left(g(\tau-t)-g(\tau+t)\right)^2\right]\cdot$$
$$\cdot\exp\left\{-i\varkappa\left[2t\left(1+\langle g^2\rangle\right)+\int_{-t}^{t}d\varphi\left(g^2(t+\tau)-\langle g^2\rangle\right)-\right.\right. \qquad (2.1)$$
$$\left.\left.-\frac{1}{2t}\left(\int_{-t}^{t}d\varphi\, g(\varphi+\tau)\right)^2\right]\right\}$$

using formula (4.2) of Ref. /7/. In the above formula $\gamma = \mathcal{E}/m$; $\alpha = 1/137$; ω is the photon frequency, $\varkappa = \frac{1}{2\omega_0\gamma^2}\frac{\omega\mathcal{E}}{\mathcal{E}-\omega}$, $\omega_0(\mathcal{E}_\perp)$ is the motion frequency; $g(\varphi)=\gamma\left[v_x(\varphi)-\langle v_x\rangle\right]$; the x-coordinate is perpendicular to the planes forming a channel; $\langle\ldots\rangle$ stands for an average value; $a(\omega) = 1+\omega^2/2\mathcal{E}(\mathcal{E}-\omega)$; and the nondipoleness parameter is $\rho = 2\langle g^2\rangle$. Formula (2.1) describes the radiation at any values of the parameter ρ, including the quantum region when the radiation recoil needs to be taken into account /1/. It should bear in mind that formula (2.1), as formula (4.2) in /7/, is straightforwardly derived from the results of Ref. /8/ which presents a quantum theory of the interaction between charged particles and a field of the plane electromagnetic wave. The total radiation probability is expressed via an imaginary part of the mass operator of a particle in the field of wave (see formula (3.36) in /8/). The frequency-differential radiation probability (spectrum) is possible to obtain using formula (3.31) of the cited publication. In this case, we are to have in mind

that the variable ' u ' is related, by virtue of eq. (2.21) in /8/, to the fourth momentum of the emitted photon k : $u=(\mathcal{A}k)/(\mathcal{A}p)$, where $\mathcal{A}$ and p are the four-momenta of the wave (of the particle). The situation under discussion corresponds to that in which a wave propagating towards an ultrarelativistic particle whose average velocity is directed along the z-axis:

$$u = \frac{\omega + k_z}{\mathcal{E} + p_z} \simeq \frac{\omega}{\mathcal{E}} \qquad (2.2)$$

Omitting the integral over u in eq. (3.31), we have the radiation probability, differential over ω, and multiplying the result by the ω, we obtain the radiation spectrum in the wave field*. The radiation under quasiperiodic motion coincides, with a quasiclassic accuracy (the terms $\sim\omega_0/\mathcal{E}$ are neglected, ω_0 is the frequency of motion), with that in a field of the corresponding wave. The vector-potential of the latter is $e\vec{A}(\mathcal{A}x)=\vec{p}(\mathcal{A}x)-\langle\vec{p}\rangle$, $eA^0=0$, e is the particle charge.

If we base ourselves on formula (3.10) in Ref. /7/, describing also the polarization properties of the radiation, then we obtain, for the radiation spectrum an expression in the form of a sum over harmonics:

$$\frac{dI}{d\omega} = \frac{\alpha\omega}{(2\pi\gamma)^2}\sum_{n=1}^{\infty}\vartheta\left(n-\varkappa\left(1+\frac{\rho}{2}\right)\right)\int_{-\pi}^{\pi}dt_1\,dt_2\,J_0\left(2\sqrt{\varkappa\left(n-\varkappa\left(1+\frac{\rho}{2}\right)\right)}\cdot\right.$$
$$\cdot\int_{t_2}^{t_1}d\varphi\, g(\varphi)\left[1+\frac{a(\omega)}{2}\left(g(t_2)-g(t_1)\right)^2\right]\exp\left\{i\left(n-\right.\right. \qquad (2.3)$$
$$\left.\left.-\frac{\varkappa\rho}{2}\right)(t_1-t_2)+i\varkappa\int_{t_2}^{t_1}d\varphi\, g^2(\varphi)\right\}$$

where J_0 is the Bessel function and $\vartheta(x)=\begin{cases}1 & x>0\\ 0 & x<0\end{cases}$; for the rest of the notations see formula (2.1). Formulae (2.1) and (2.3) are completely equivalent and describe the radiation from both the electrons and positrons. To derive explicit expressions, it is necessary to find $v_x(\varphi)$, i.e. to solve the problem of one-dimensional motion. This is possible in any potential.

---

* This procedure is permissible because no integration by parts over the variable u has been made when deriving formula (3.31).

In what follows, we shall make a comparison between the radiation of electrons and positrons. For the positron case, a parabolic potential has been used in Ref. /5/, and for electrons it corresponds to a 'inverse parabola' potential which well describes the electron motion. For the more suitable potential introduced in /10/, the expressions for v_x, derived in Refs. /1,10/ should be used.

In the parabolic ('inverse parabola' for electrons) potential we have, from (2.3) for the radiation spectrum at a given energy $\varepsilon_\perp$

$$\frac{dI}{d\omega} = -\frac{\alpha}{\pi^2 d}\vartheta_c \xi_0\left(1-\frac{\omega}{\varepsilon}\right)\sum_{n=1}^{\infty}\vartheta\left(\frac{n}{s}-\xi_0\left(1+\frac{\rho}{2}\right)\right)\cdot$$
$$\cdot\int_{-\pi}^{\pi} dt_1 dt_2\, J_0\left(2\sqrt{\rho_0\xi_0\left(\frac{n}{s}-\xi_0\left(1+\frac{\rho}{2}\right)\right)}(q_1-q_2)\right)\cdot \qquad (2.4)$$
$$\cdot\left[1+\frac{\rho_0 a(\omega)}{2}(\psi_1-\psi_2)^2\right]\cos\left[n(t_1-t_2)+\frac{\xi_0\rho_0}{2}(z_1-z_2)\right],$$

where $\xi_0=\omega/2\gamma^2\omega_{0s}\left(1-\frac{\omega}{\varepsilon}\right)$, ω_{0s} is the $\varepsilon_\perp$-independent frequency of motion in the parabolic potential: $\omega_{0s}=\frac{2}{d}\vartheta_c$, d is the distance between planes forming the channel, $s=T/T_{0s}$, T is the period of motion, $T_{0s}=2\pi/\omega_{0s}$; index $(1,2)$ indicates the dependence of the function on t_1 or t_2. The explicit expressions for the $q_y(t)$, $\psi(t)$ and $z(t)$ functions are given in Table I for $t>0$; at $t<0$ we have $\psi(-t)=\psi(t)$, $q_y(-t)=-q_y(t)$ and $z(t)=-z(t)$; the Table also presents $S=S(\xi)$ and $\rho(\xi)$. The variable ξ is equal to $\varepsilon_\perp/u_0$; index 'c' is for the particles in the channel $(\xi<1)$ and index "nc" is referred to the particles $(\xi>1)$ above the barrier; the following notations have been introduced:

$$S(\xi)=\frac{1}{2}\ln\left|\frac{\sqrt{\xi}+1}{\sqrt{\xi}-1}\right| \text{ and } A(\xi)=\arcsin\frac{1}{\sqrt{\xi}}.$$

With an increase of ξ from 0 to 1 the motion period of an electron in channel increases and above the barrier decreases monotonously and at $\xi\gg1$, $T\sim1/\sqrt{\xi}$; in the vicinity of the point $\xi=1$ the period $T\sim-\ln|1-\xi|$. The parameter $\rho(\xi)$ increases in the channel with growing ξ, attains a maximum, $0.43\,\rho_0$ at $\xi\simeq0.85$, and then reduces to 0. Above the barrier, $\rho(\xi)$ grows from 0, takes the value $\rho^{nc}_{max}\simeq\rho_0\cdot 0.13$ at $\xi\simeq1.001$, then decreases, and $\rho/\rho_0\simeq2/45\xi$ at $\xi\gg1$. This result coincides with that for the positron case because $\rho\simeq\gamma^2(u^2-\langle u^2\rangle)/\varepsilon\varepsilon_\perp$ highly above the barrier and is independent of the charge sign of particle. In general,

with $\xi\gg1$ the radiation does not depend of the sign of charge (see, e.g., Section 4 in Ref. /1/), since in this limit the result coincides with the Born approximation. Recall (see Ref. /9/) that the total electron radiation intensity in the potential under consideration is

$$I(\xi)=I_e\left(1-\xi+\frac{\sqrt{\xi}}{f(\xi)}\right) \qquad (2.5)$$

where $I_e=\frac{16e^2u_0^2\gamma^2}{3m^2d^2}$, it decreases from $2I_e$ at $\xi=0$ to 0 at $\xi=1$, and then increases, at $\xi>1$, approaching $I_{as}=\frac{2}{3}I_e$.

Formulae (2.1), (2.3) and (2.4) may be used for any ρ_0. In case of a moderate nondipoleness ($\rho_0\sim1$), the condition $\rho\ll1$ is satisfied for the above-barrier electrons, and it is possible to describe their radiation using the dipole formulae which are considerably simpler (cf. /5/). At $\rho_0\sim1$, the description of the radiation from electrons in the channel can be made significantly simpler as well. The velocity $v_x(\varphi)$ (just as the function $q(\varphi)$) in (2.1) can be expanded in Fourier series

$$v_x(\varphi)=\sum_{l=1}^{\infty}v_{2l-1}\cos\left((2l-1)\varphi\right) \qquad (2.6)$$
$$v_{2l-1}=\frac{1}{\pi}\int_0^{2\pi}d\varphi\, v(\varphi)\cos\left((2l-1)\varphi\right)$$

The values of v_{2l-1} for appropriate potentials are given in Refs. /1/ and /9/. The quantity v_{2l-1} falls as the motion harmonic l grows, and the corresponding radiation frequency shifts to the right. Thus, the contribution of the higher motion harmonics l to the region of a maximum of the resultant spectrum ($\xi\sim1$) proves to be suppressed for two reasons: 1) we have found ourselves on the left slope of the curve for a given l and 2) even in its maximum the harmonic l contributes much less as compared with the first harmonic at $\xi\sim1$. Correspondingly, at $\xi\sim1$, for the purpose of describing the radiation from channeled particles one can restrict oneself to a few terms in (2.6). If we retain only the first term $v_1\cos\varphi$ in (2.6), then substituting an appropriate $g(\varphi)$ into (2.1) we

are led to formula (4.6) from Ref. /7/ , wherein the following substitution should be made: $\rho \to \rho_1 = \gamma^2 v_1^2$. We also present here an expression for the spectrum with taking into account also a small addition contributed by the term $v_3 \cos 3\varphi$

$$\frac{dI}{d\omega} = \frac{i\alpha\omega}{2\pi\gamma^2} \int_{-\infty}^{\infty} \frac{dt}{t-i0} e^{-i z_1} \Big[J_0(z_0) + a(\omega)\rho_1 \sin^2 t \cdot \tag{2.7}$$

$$\cdot \left(J_0(z_0) - i J_1(z_0) \right) + \rho_1 \frac{v_3}{v_1} G(t) \Big]$$

where

$$G(t) = 2a(\omega) \sin t \sin 3t \left(J_2(z_0) + i J_1(z_0) \right) + \varkappa \left(\sin 2t - \right.$$

$$\left. - 2 \sin t \sin 3t / 3t \right) \left[b J_1(z_0) + i (b-1) J_1'(z_0) \right] + \varkappa^2 \left(\sin 2t \cos 2t - \right. \tag{2.8}$$

$$\left. - 2 \sin t \sin 3t / 3t \right) \left[i b J_2(z_0) - (b-1) J_2'(z_0) \right],$$

$b = 1 + \rho_1 a(\omega) \sin^2 t$, $z_0 = \varkappa \rho_1 \left(\frac{\sin^2 t}{t} - \frac{\sin 2t}{2} \right)$, $z_1 = 2t\varkappa \left(1 + \frac{\rho_1}{2} \right) - \varkappa \rho_1 \frac{\sin^2 t}{t}$

To make better the convergence of the integral in (2.7), one can use the subtraction procedure described in /7/.

The presented approach calls for a knowledge only of the Fourier harmonics of velocity and, hence, is applicable to the description of radiation from both the electrons and positrons in any potential. We note that the dependence $T(\varepsilon_\perp)$ is taken into account exactly and the quantity ρ_1 is close to ρ . Since for electrons at $\varkappa \to 1$ the period $T(\varkappa)$ tends to infinity in any adequate potential, the non-harmonicity of motion will be largest at $\varkappa \to 1$. So, in the 'inverse parabola' potential, with $\varkappa$ = (0.3; 0.6 and 0.9) the v_3/v_1 is equal, correspondingly, to 0.13; 0.15 and 0.22 and v_5/v_1 = = (0.045; 0.056 and 0.089). However, because at $\varkappa \to 1$ the intensity (2.5) $I(\varkappa) \to 0$, the radiation from the particles which have undergone a significant non-harmonic motion, may be neglected at a finite population at $\varkappa \to 1$. Even in the case when the population in the channel is $\sim f(\varkappa)$ (thin crystal, the particles are uniformly distributed over the angle of incidence $\vartheta_0 \leq \vartheta_c$; very thick crystal) and $I(\varkappa) f(\varkappa) \to I_e$ at $\varkappa \to 1$, a fraction of particles in the vicinity of $\varkappa = 1$ is small and their radiation lies within low frequencies.

3. Analysis of the radiation in thin crystals

Dechanneling in thin crystals may be neglected by definition and the distribution over $\varepsilon_\perp$ is determined by the initial conditions. If the incident beam is uniformly distributed within the $\vartheta_1^\circ \div \vartheta_2^\circ$ interval, then in the 'inverse parabola' potential we have (see, e.g., formula (A.4) in /1/)

$$\frac{dN}{d\varkappa} = \frac{\vartheta(\varkappa - y_1^2)\,\vartheta(1 + y_2^2 - \varkappa)}{2(y_2 - y_1)} \ln \frac{C}{B} \tag{3.1}$$

where $y_{1,2} = \frac{1}{\vartheta_c} \vartheta_{1,2}^\circ$, $C = (1+\sqrt{\varkappa})\,\vartheta(y_2^2 - \varkappa) + (y_2 + \sqrt{1 + y_2^2 - \varkappa}) \cdot$

$\cdot\, \vartheta(\varkappa - y_2^2)$, $B = (y_1 + \sqrt{1 + y_1^2 - \varkappa})\,\vartheta(1 + y_1^2 - \varkappa) + \sqrt{\varkappa - 1} \cdot$

$\cdot\, \vartheta(\varkappa - 1 - y_1^2)$

The spectra $dI/d\omega$, averaged with $dN/d\varkappa$ (see formula (3.1)), are presented in Figs. 1-4 wherein the frequency is laid off in the units of $\varkappa_0$. Figures 1-3 demonstrate the spectra in Si ((110) plane at $\mathcal{E}$ = 10 GeV; $\varkappa_0 = 1$ corresponds to ω = 110 MeV for the intervals of the incident angles (0-20) μrad (Fig. 1), (0.-50) μrad (Fig. 2) and of (40-60) μrad (Fig. 3); the Lindhard angle is ϑ_c = 71 μrad. Figure 4 illustrates the spectra in diamond ((110) plane), $\mathcal{E}$ = 4.3 GeV ($\varkappa_0 = 1$ corresponds to ω = 50 MeV, ϑ_c = 113 μrad, ρ_0 = 0.9) for the (-90 ÷ 90), (0 ÷ 180) and (90-270) μrad intervals of angles. In Figure 1, for the curve (a) the $dI_{nc}/d\omega$ has been calculated by means of the dipole formulae (see Refs. /9/), and the $dI_c/d\omega$ has been calculated according to formula (2.7); (with the term $\sim v_3$ omitted). Curve (b) is a result of calculations by means of the exact formula (2.4). It is seen that taking into account only one harmonic of motion (at a given $\varepsilon_\perp$) is a good approximation. In addition, the discrepancy between curves (a) and (b) is more noticeable on their right slope. For comparison, we also present the radiation spectrum for positrons (curve (c)) obtained under the same conditions in Ref. /5/. Just as in the dipole case, the spectral curve for electrons is wider and has a less height in its maximum (cf. Refs. /1,9,10/) when comparing with that for positrons, al-

though the difference in height in the nondipole region becomes not so significant. Curve (a) (Fig. 2) shows that the broadening of the incident beam (compare with Fig. 1(a)) results lowering the height of the maximum, because the amount of particles in the channel decreases, and this is the particles which contribute to the spectrum in the region of maximum. In addition, the fraction of the above-barrier particles whose spectrum is represented by curve (a') is also increased. This circumstance is one of the reasons for which the maximum of the summary curve (a), calculated by means of eq. (2.7), shifts to the right. Figure 2 also shows the results of the calculation, made by means of eq. (2.4), (curve b) and the radiation spectrum for positrons from Ref. /5/ (curve c). It is seen from Fig. 3 that the rotation of the narrow beam by the angle $\sim \vartheta_c$ leads to sweeping changes in the spectrum. The channeled (a'') and above-barrier (a') particles contribute on different frequencies and their contributions are approximately equal in magnitude; as a consequence, the summary spectrum (a) has a wide plateau. The corresponding spectrum for positrons /5/ is shown by curve (c). Figure 4 demonstrates that when rotating a wide beam by an angle of about $\sim \vartheta_c$ a maximum (keeping its position) from the channeled particles is still clearly seen in the radiation spectrum.

Reference /5/ has indicated the simple rules to find the characteristic points (maxima and minima) on the spectral curve for positrons, which are based on an analysis of the z --dependence of the intensity and of the argument of ν -functions in (2.4). For electrons these structures are washed out on account of a large width of the spectral curves which is due to a substantial spread of the motion periods. The estimates become less definite as a result. The spectral curve has, as a rule, one maximum which is due to the first harmonic (term with n = 1 in (2.4)) of radiation from the channeled particles (in Figs. 1,2,4 this maximum is at $\xi_0 \sim 1$). It follows from (2.4) that at $n = 1$ the radiation frequencies lie within the interval $(0 \le \xi_0 \le \xi_1, \xi_1 = \frac{1}{S(1+\rho/2)})$. The quantity $S(1+\rho/2)$ grows monotonously with increasing z $(0<z<1)$, and ξ_1 shifts to the left with increasing z. For estimation, it is convenient to introduce a 'weighted intensity': $F(z) = I(z)\frac{dN}{dz}$. If

$\max F = F(z_1)$, then as z increases from 0 to z_1 the boundary frequency shifts to the left and the peak becomes higher ($\sim F(z)$). At larger z both functions $F(z)$ and ξ_1 fall off. As a result, the maximum of the resultant distribution $dI_c/d\omega$ lies to the left from the point $\xi_m^c(z_1) = 1/S(z_1)(1+\rho(z_1)/2)$. If the function $F(z)$ has a sharp peak at z_1, then the maximum $dI_c/d\omega$ will lie near $\xi_m^c(z_1)$. If at $z>1$, $\max F(z) = F(z_2)$, then, similarly, the maximum of $\frac{dI_{nc}}{d\omega}$ is to the left from $\xi_m^{nc}(z_2) = 1/S(z_2)\left(1+\frac{\rho(z_2)}{2}\right)$. For illustration, we consider the case when a narrow beam is incident at ϑ_0 near ϑ_c (Fig. 3). Here the function $F(z)$ has a clear maximum both in the channel ($z_1 \simeq 0.7$) and above the barrier ($z_2 \simeq 1.4$); the corresponding frequencies are: $\xi_m^c \simeq 0.94$ and $\xi_m^{nc} \simeq 2.4$. In Fig. 3 the maxima of the spectral curves correspond to $\xi_{max}^c \simeq 0.8$ and $\xi_{max}^{nc} \simeq 2.1$. We would like also to discuss an important case when $dN/dz \sim f(z)$. As shown in Ref. /11/, such a distributior is established in thick crystals in the channel and above the barrier at not too large $z = \varepsilon_1/u_0$. This case is realized in thin crystals if $0 \le \vartheta_0 \le \vartheta_c$ (see eq. (3.1)); whereas if $0 \le \vartheta_0 \lesssim \vartheta_c$, then the distribution is not strongly different, in configuration, from $f(z)$. The function $F(z) = I(z)f(z)$ has a maximum at $z_1 \simeq 0.695$, and $\xi_m^c(z_1) \simeq \frac{1.3}{1+\rho_0/5}$. For the (110) plane, at ε = 10 GeV $\xi_m^c \simeq 0.94$ in Si, and at ε = 4.3 GeV $\xi_m^c \simeq 1.1$ in diamond (cf. Figs. 1,2,4; curve (a)).

4. Radiation in thick crystals

For a thick crystal, the thickness is $L \gg l_d$, where l_d is the dechanneling length, introduced in /1/:

$$l_d = \frac{\alpha}{2\pi}\rho_0 L_{rad} \qquad (4.1)$$

Here L_{rad} is the radiation length in an apprcpriate amorphous medium. If $\varepsilon \lesssim 10^{11}$ eV, then multiple scattering will dominate in evolution of the distribution function (DF) over $\varepsilon_\perp$ (see Ref. /11/). We shall take this evolution account just as in Ref. /12/, assuming that the incident beam is a Gaussian one with respect to the incident angles (its width is Δ_c). Namely we write down the initial distribution in which the

substitution $\Delta_0^2 \to \Delta_0^2 + \vartheta_s^2(l)/2$ is made ($\vartheta_s^2(l)$ is the average squared angle of multiple scattering in an appropriate amorphous medium* at a depth l). If the channeling radiation is not collimated, then one can obtain the distribution over z, averaged over the crystal thickness, from formula (4) in Ref. /12/ where it is necessary to make an elementary integration over ν :

$$\left\langle \frac{dN}{dz} \right\rangle = \frac{1}{L}\int_0^L \frac{dN(l)}{dz}\,dl = \sqrt{\frac{2}{\pi\lambda}}\,\frac{1}{1-\beta}\left\{ f(z)\left[e^{-\frac{z}{2\lambda}} - \sqrt{\beta}\,e^{-\frac{z}{2\tilde{\Delta}_0^2}}\right] - \frac{1}{\lambda}\int_{\sqrt{z}}^{\sqrt{z/\beta}} du\, e^{-\frac{u^2}{2\lambda}} + \frac{1}{\sqrt{\lambda}}\int_0^{f(z)} du\, g_1 \cdot \right.$$
$$\left. \cdot (u g_2 - g_1)\left[\frac{1}{\sqrt{\lambda}}\,e^{-\frac{g_2^2}{2\lambda}} - \frac{1}{\tilde{\Delta}_0}\,e^{-\frac{g_2^2}{2\tilde{\Delta}_0^2}}\right]\right\} \qquad (4.2)$$

where

$$\lambda = \frac{L}{l_d} + \tilde{\Delta}_0^2\,, \quad \tilde{\Delta}_0 = \frac{\Delta_0}{\vartheta_c}\,, \quad \beta = \frac{\tilde{\Delta}_0^2}{\lambda}\,, \quad g_2(u) = \frac{dg_1}{du},$$

$$g_1(u) = \sqrt{|1-z|}\left\{\vartheta(1-z)\operatorname{ch} u + \vartheta(z-1)\sin u\right\} \qquad (4.3)$$

From (4.2), there is no difficulty in deriving an asymptotic distribution at $L \gg l_d$. In this limit, $\beta \to 0$ and $\lambda \to \infty$, and we find, within an accuracy up to the terms, $\sim 1/\sqrt{\lambda}$

$$\left\langle \frac{dN}{dz} \right\rangle = \sqrt{\frac{2 l_d}{\pi L}}\, f(z)\, e^{-\frac{z}{2\lambda}} \qquad (4.4)$$

so that for $z \ll \lambda$ we have $\left\langle \frac{dN}{dz} \right\rangle \sim f(z)$. An analysis of the solution of the kinetic equation, which was made in Ref. /11/, has shown in a general form that at very large depths this distribution corresponds to an uniform one in transverse phase space. Thus, at $L \to 0$ the expression (4.2) is exact (for the Gaussian beam) and has a correct asymptotics at $L \to \infty$. This permits one to hope for a satisfactory description of the function $\langle dN/dz \rangle$ at any l.

---

* In an adiabatic approximation, the energy losses may be taken into account in $\vartheta_s^2(l)$ (Ref. /13/).

In the foregoing, we have estimated the position of the maximum of the spectral curve at $L \gg l_d$. Let us now show that these curves prove to be similar at different (large) thicknesses. Indeed, the resultant spectrum is given by an integral

$$\int_0^\infty \left\langle \frac{dN}{dz} \right\rangle \frac{dI}{d\omega}\, dz \qquad (4.5)$$

Consider now the case of large L when it is possible to use eq. (4.4). We split the integration region into two parts: $0 \div z_0$ and $z_0 \div \infty$; with $1 \ll z_0 \ll \lambda$. After that, in the first part one can substitute $\exp(-z/2\lambda) \to 1$ and we obtain a contribution, including L, only as the factor $L^{-1/2}$. It is the region ($z \sim 1$) that contributes to the maximum of the spectrum ($\varkappa_0 \sim 1$). In the second part ($z \gg 1$) the particles are in the high-lying above-barrier states and the dipole formulae may be used. Making use of formula (7) in Ref. /9/, we have roughly, at $z \gg 1$: $dI/d\omega \sim \frac{\varkappa_0}{z}$ (photons with a frequency up to $\varkappa_0 \sim 2\sqrt{z}$ are emitted). Although the contribution of these particles breaks the similarity, it is strongly suppressed at $\varkappa_0 \sim 1$. The region up to $z \sim \lambda$ contributes to the integral $\int_{z_0}^{\infty} dz$, so that the frequency boundary of the spectrum corresponds to $\varkappa_0 \sim 2\sqrt{\lambda}$. So, at $\varkappa_0 \sim 1$ the shape of the spectrum proves to be universal, and the difference in height is determined by the scale factor* $\sim L^{-1/2}$. The accuracy of this expression is not worse than $\lambda^{-1/2}$ (the order of the terms omitted in going from (4.2) to (4.4).

As an illustration, we shall analyse the radiation from electrons upon channeling in the plane (110) of a diamond monocrystal with the thickness $L_1 = 0.1$ mm (Fig. 5), $L_2 = 1$ mm (Fig. 6) and $L_3 = 1.7$ mm (Fig. 7) at $\mathcal{E} = 4.5$ GeV; then $\vartheta_c \simeq 110$ μrad, $\rho_0 \simeq 0.95$ and at $\omega = 54$ MeV $\varkappa_0 = 1$; this corresponds to the experimental conditions /14/. The authors

---

* Upon collimation of the photon beam to an angle $\lesssim \vartheta_c$ the factor $\sim \frac{1}{L}\ln\frac{L}{l_d}$ arises. Recall that all the formulae incorporate the intensity recalculated per unit length.

of the cited publication estimate the angular width of the incident beam as $\Delta_0 \simeq 60\mu$rad. Theoretical curves (1) in Figs. 5-7 are the sum of the contributions from the radiation in a continuous potential of the planes; ($\langle dN/dz \rangle$ is taken in the form (4.2)) and the bremsstrahlung* (the latter contribution is depicted as the dotted line; as seen, it is negligibly small). The crystals L_2 and L_3 are thick enough; for them (see eq. (4.2)) λ is: $\lambda_2 = 7.7$, $\lambda_3 = 13$. The expected accuracy of the similarity of the spectral curves will be about $\sim \lambda^{-1/2}$ (30-40%) and asymptotic scale factor is $(L_2/L_3)^{-1/2} \simeq 1.3$. For $\chi_0 \leq 2$ neglecting bremsstrahlung the calculated curves in Figs. 6,7 are similar within an accuracy better than 5% and the scale factor is 1.2; Its difference from $(L_2/L_3)^{-1/2}$ means that the asymptotic regime does not yet occur. Nevertheless, the accuracy of similarity, at $\chi_0 \lesssim 2$, has proved to be much better than the estimate with respect to $\lambda^{-1/2}$. Curves (2) in Figs. 5-7 are the contribution given by the above-barrier particles. As the thicknesses grow, the maxima on them shift to the right, while the maximum in the contribution of the channeled particles ($\chi_0 \simeq 0.8$) remains unchanged. The maximum in the resultant spectrum remains practically at the same place (curves I).

Figures 5-7 also present the experimental data (Ref. /14/). For a sample with $L_1 = 0.1$ mm, the theory and experiment agree quite well at $\chi_0 \leq 2$. However, for the thicker samples the maximum of the experimental spectrum shifts to the right. The authors /14/ account for this by multiple scattering and by the peculiarities of the spectrometer detecting two or more simultaneously emitted photons as one photon with the summed energy. Since we have made allowance for multiple scattering, the reason for the difference with the theory may be in fact associated with the specific features of the detector in Ref. /14/. The probability of emission of a photon with frequency $\chi_0 \leq 2$ can be evaluated using the spectral curves in Figs. 5-7; for the samples with L_1, L_2 and L_3 we have, correspondingly; $W \simeq$ (0.08; 0.46 and 0.65) so that the probability of simultaneous emission of two photons is not small for L_2 and L_3.

---

* We describe bremsstrahlung using the standard formulae.

The accuracy of the dipole approximation is possible to estimate by calculation in this approximation and by means of exact formulae. Consider the radiation in the (100) plane in Si at $\mathcal{E} = 1.2$ GeV ($\vartheta_c = 150\,\mu$rad, $\rho_0 \simeq 0.13$; $\chi_0 = 1$ corresponds to $\omega = 4.8$ MeV); at $L = 0.24$ mm, $\Delta_0 \simeq 100\mu$rad that is in accord with the experimental conditions /15/. The calculation with the use of formula (4.2) are given in Fig. 8 where (1) is the contribution from the channeled particles, (2) is the contribution given by the above-barrier particles, the dotted line is for the contribution of the bremsstrahlung, and curve (3) shows the sum of all these contributions. In the dipole approximation, the radiation has been calculated using the formulae from Ref. /12/. Since in Ref. /15/ the photons have not been collimated, but the expressions in Ref. /12/ incorporate the collimation, the spectrum has been calculated for a set of increasing collimation angles Δ_{col}; starting with $\Delta_{col} \sim \frac{4}{\gamma}$ the shape of the spectrum practically stops changing (cf. the discussion in /11/) because nearly all the particles radiate to the collimator in this case. Comparison with curves (1) and (2) in Fig. 8 has shown that the dipole curves lie 5-10% higher ($\sim \rho_0$). We would like to attract the reader's attention to the fact that the shape of the spectrum in Fig. 8 is mainly determined, in the region of maximum, by the contribution of the particles in the channel. The above-barrier particles give a dominant contribution only on the right slope (at $\chi_0 > 2$). This is inconsistent with the assertion in /15/ that taking into account the contribution of the above-barrier particles only is a good approximation. Note a good agreement of the theory, free from fitted parameters, with the experiment /15/ (unlike the theoretical arguments in /15/).

In Ref. /16/, the radiation from the electrons with energy $\mathcal{E} = 4.3$ GeV has been measured in a diamond with the thickness $L_4 = 0.1$ mm ((0 11) plane) and $L_5 = 0.47$ mm (index 'a' denotes the (011) plane and 'b' stands for the (001) plane) for which $\vartheta_{c\,a(b)} = 113(79)\,\mu$rad and $\rho_{0\,a(b)} = 0.91(0.44)$; at $\chi_0 = 1$, $\omega_{a(b)} = 50(49)$ MeV. The divergence of the incident beam was $\Delta_0 \simeq 100\,\mu$rad (Ref. /16/) and the beam of radiated photons

was collimated to a solid angle of 10^{-7} ster*. The measured dependence /16/ of the spectrum on the incident angle is qualitatively similar to that in Fig. 4 where the collimation and dechanneling were not taken into account. In Ref. /12/ the radiations has been studied for the case of the photon-beam collimation. For the nondipole region, the calculations can be made in the same manner, but become much more timeconsuming. We use here a simpler approach with regard for the concrete experimental conditions of Ref. /16/. Since $\vartheta_c < \vartheta_{col}$, the radiation from the channeled particles will not arrive at the collimator if the transverse velocity component turns out to be too large: $v_y > \vartheta_{col}$. Within the frame of the accepted multiple-scattering model it is easy to find a fraction of particles with $v_y < \vartheta_{col}$: $k_4 \simeq 0.88$ and $k_5 \simeq 0.72$. If $\vartheta_c < \vartheta_{col}$, then the collimator will cause the deformation of the radiation spectrum only in the region of low frequencies. So, we multiply the spectral radiation-intensity distribution $dI_c/d\omega$ by the coefficients $k_4(k_5)$ (curves (1)) in Figs. 9-11) and add to them $dI_{nc}/d\omega$ calculated using the dipole formulae ($\rho_0 < 1$) Ref. /12/ (curve (2) in Figs. 9-11); curve (3) gives the total contribution (without the allowance for the bremsstrahlung constituting a few percent). Curve (4) in Fig. 11 presents the spectrum calculated according to Ref. /12/. From the above analysis the accuracy of the dipole approximation is roughly 20-30% under these conditions ($\rho_0 \simeq 0.44$). Comparison of the curves (3) and (4) in Fig. 11 shows that the used procedure somewhat changes the shape of the spectrum on the left slope. The difference constitutes 20% in the peak region and on the right slope. For a disoriented crystal, the influence of the collimator can be taken into account in a similar way; then $k_4^{br}(k_5^{br}) \simeq 0.71$ (046), and at $\omega \ll \mathcal{E}$ the spectrum is $dI^{br}/d\omega \simeq \frac{4}{3L_{rad}} k_4^{br}(k_5^{br})$. The results in Ref. /16/ are represented in terms of $d(I_c+I_{nc})/dI^{br}$. We give then in an absolute normalization using the indicated value of $\frac{dI^{br}}{d\omega}$ in Figs 9-11.

---

* We thank A.O.Aganiants for discussion of the conditions of the experiment.

In Refs. /17/ and /18/ the authors have analysed the radiation at channeling electrons in the (110) plane of a silicon crystal at the energy $\mathcal{E}$ = 10 GeV and $\mathcal{E}$ = 7 GeV, respectively. The crystal thickness was L_1 = 0.135 mm (Ref. /17/ and L_2 = 0.1 mm (Ref. /18/); $\vartheta_c^{1(2)}$ = 71 (95) μrad, $\rho_0^{1(2)} \simeq 1.9(1.33)$; $\xi_0 = 1$ corresponds to $\omega^{1(2)}$ = 110(65) MeV. In Ref. /17/, the events with $\vartheta_0 \leq 50\,\mu$rad have been detected and the accuracy of measuring the angles is also estimated in 50 μrad. Therefore, we put $\Delta_0 = 100\,\mu$rad, bearing in mind the notes of Ref. /18/ about the experimental set up in Ref. /17/, the quantity Δ_0 in Ref. /18/ was $\Delta_0 \simeq 60$ rad. Figures 12 and 13 give the calculational results and experimental data for $\mathcal{E}$ = 10 GeV (Ref. /17/) and $\mathcal{E}$ = 7 GeV (Ref. /18/) which we have represented in absolute units.

Thus, we can see that the developed theory of radiation from electrons at planar channeling, not containing the fitting parameters, describes quite well the experiments for various media, planes and thicknesses in a broad interval of energies. It follows from this, in particular, that the used simple dechanneling model is quite adequate.

References

1. V.N.Baier, V.M.Katkov, V.M.Strakhovenko. Radiation of Relativistic Particles at Planar Channeling. Preprint of the INP 80-03, Novosibirsk, 1980 (in Russian).
2. M.A.Kumakhov, Ch.G.Trikalinos, phys. stat. sol. (b) 99, 440 (1980).
3. V.A.Bazylev, V.I.Glebov and N.K.Zhevago. Soviet Phys., - - J. exper. theor. Phys. 51, 31 (1980).
4. N.F.Shulga, L.E.Gendenstein, I.I.Miroshnichenko et al. Zh. Exp. Theor. Fiz. 82, 501 (1982).
5. V.N.Baier, V.M.Katkov, V.M.Strakhovenko. Dokl. Akad. Nauk SSSR, 266, 605 (1982); Preprint INP 81-139, Novosibirsk, 1981.
6. V.A.Bazylev, V.V.Beloshitskii, V.I.Glebov et al. Zh. Eksp. Theor. Fiz. 80, 608 (1981).
7. V.N.Baier, V.M.Katkov, V.M.Strakhovenko. Soviet Phys. - - J. exper. theor. Phys. 53, 688 (1981).
8. V.N.Baier, V.M.Katkov, A.I.Milstein, V.M.Strakhovenko. Soviet Phys. - J. exper. theor. Phys. 42, 400 (1975).
9. V.N.Baier, V.M.Katkov, V.M.Strakhovenko. Soviet Phys., - - Doklady 24, 469 (1979).
10. V.N.Baier, V.M.Katkov, V.M.Strakhovenko. Phys. Letters A73, 414 (1979).
11. V.N.Baier, V.M.Katkov, V.M.Strakhovenko. Phys. stat. sol. (6) 118, 499 (1983).
12. V.N.Baier, V.M.Katkov, V.M.Strakhovenko. Dokl. Acad. Nauk SSSR 268, 1365 (1983).
13. V.N.Baier, V.M.Katkov, V.M.Strakhovenko. Dokl. Acad. Nauk, SSSR 275, 1369 (1984).
14. R.O.Avakyan, E.O.Avakyan, A.E.Avetisyan et al. 2nd All Union conference on Radiation of Relativistic Particles in crystals Gheget. 1982.
15. V.B. Ganenko, N.N.Nasonov, E.V.Peguschin et al. Ukran. Fiz. Zh. 28, 302 (1983).

16. A.O.Aganiants, Yu.V.Vartanov, H.A.Vartapetyan et al. Angular Dependence of 4.3 GeV Electrons Radiation Spectra at Small Angles of Entry into Diamond Single Crystals. Preprint of YPI-666(56)-83, Yerevan (1983).
17. M.Atkinson, J.F.Bock, P.J.Bassey et al. Radiation from planar channeled 5-55 GeV/c positrons and electrons. CERN--EP/82-03(1982).
18. J.Back, F.Komarov, Ph.Meyer et al. Measurement of channeling radiation and its polarization and X-ray excitation, together with deviation from Zanday distribution. CERN/PSCC/82-94 (1982).

Table 1

The functions involved in the formula (2.4)

Particles and type of motion / Function	e_c^+	e_{nc}^+	e_c^-	e_{nc}^-
$\Psi(t)$	$\sqrt{z}\cos(st)$		$\sqrt{z}\,ch\,st - sh\,st$	
$q_1(t)$	$\sqrt{z}\sin t$	$\sqrt{z}\sin st - \frac{t}{\pi}$	$1 - ch\,st + \sqrt{z}\,sh\,st$	$1 - ch\,st + \sqrt{z}\,sh\,st - \frac{t}{\pi}$
$\tau(t)$	$\frac{1}{2}z\sin 2t$	$\frac{1}{2}\sin 2st - \frac{4q_1(t)}{\pi s} - \frac{t}{\pi}\sqrt{z-1}$	$\sqrt{z}(1-ch\,2st) - \frac{2\pm\sqrt{z}}{\pi} + \frac{1+z}{2}sh\,2st$	$\sqrt{z}(1-ch\,2st) + \frac{1+z}{2}sh\,2st - \frac{t}{\pi}\sqrt{z} - \frac{4}{\pi s}q_1(t)$
$S(z)$	1	A/π	$2f/\pi$	f/π
$\frac{\rho(z)}{\rho_0}$	z	$z + \frac{\sqrt{z-1}}{A} - \frac{2}{A^2}$	$z + \frac{\sqrt{z}}{f} - 1$	$z + \frac{\sqrt{z}}{f} - 1 - \frac{2}{f^2}$

Figure captions

Fig. 1. Spectral intensity of radiation from electrons with $\mathcal{E}$ = 10 GeV upon their motion along the (110) plane of the Si crystal when the initial beam is uniformly distributed over the angle of incidence in the 0÷20 μrad.
Curve (a) is for the calculation by means of formula (2.7) at $\nu_3 = 0$, curve (b) is calculation using formula (2,4) and curve (c) is for the positron spectrum under the same conditions. The value of $\tilde{\varepsilon}_0 = 1$ corresponds to the energy ω = 110 MeV.

Fig. 2. The same as in Fig. 1 for the 0÷50 μrad angles of incidence. Curve (a') is the contribution of the above-barrier electrons.

Fig. 3. The same as in Figs. 1,2 for the 40÷60 μrad angles of incidence. Curve (a'') shows the contribution from the channeled electrons.

Fig. 4. Spectral intensity of radiation from electrons with $\mathcal{E}$ = 4.3 GeV upon motion along the (110) plane in a diamond when the initial beam is uniformly distributed over the angle of incidence in the -90÷90 μrad (curve 1) 0÷180 μrad, (curve 2) and 90÷270 μrad (curve 3) interval. The value of $\tilde{\varepsilon}_0 = 1$ corresponds to the energy ω = 50 MeV.

Fig. 5. Spectral intensity of radiation, per unit thickness, from electrons with $\mathcal{E}$ = 4.5 GeV upon motion along the (110) plane in a diamond whose thickness is L_1 = 0.1 mm. The value of $\tilde{\varepsilon}_0 = 1$ corresponds to ω = 54 MeV. The dotted line shows the bremsstrahlung contribution, curve (2) is the contribution of the above-barrier electrons and curve (1) is the resultant spectrum; the experimental data are from Ref. /14/.

Fig. 6. The same as in Fig. 5 for the crystal thickness L_2 = 1 mm.

Fig. 7. The same as in Fig. 6 for the crystal thickness L_3 = 1.7 mm.

Fig. 8. Spectral intensity of radiation, per unit thickness, from electrons with $\mathcal{E}$ = 1.2 GeV upon motion along the (100) plane in the Si crystal of L_1 = 0.24 mm. The value of ξ_0 = 1 corresponds to ω = 4.8 MeV. The bremsstrahlung contribution is shown by the dotted line. Curve (1) is the contribution from the channeled electrons, curve (2) is that from the above-barrier ones, and curve (3) is the resultant spectrum; the experimental data are from Ref. /15/.

Fig. 9. Spectral intensity of radiation, per unit thickness, from the electrons with $\mathcal{E}$ = 4.3 GeV upon their motion along the (011) plane of a diamond crystal with L_4 = 0.1 mm. The value of ξ_0 = 1 corresponds to ω = 50 MeV. Curve (1) is the contribution of the channeled electrons, curve (2) is that of the above-barrier ones, and curve (3) is the summed contribution without the bremsstrahlung taken into account; the experimental data have been taken from Ref. /16/.

Fig.10. The same as in Fig. 9 for the crystal thickness L_5 = 0.47 mm.

Fig.11. The same as in Fig. 10 for the (001) plane. The value of ξ_0 = 1 corresponds to the energy ω = 49 MeV. Curve (4) is the result of calculation by means of formulae in Ref. /12/.

Fig.12. Spectral intensity of radiation, per unit thickness, from the electrons with $\mathcal{E}$ = 10 GeV upon motion along the (110) plane of a Si crystal of L = 0.135 mm; the experimental data have been taken from Ref. /17/. The value of ξ_0 = 1 corresponds to ω = 110 MeV. The dotted line shows the bremsstrahlung. The solid curve is a summed spectrum.

Fig.13. The same as in Fig. 12 for $\mathcal{E}$ = 7 GeV and crystal thickness L = 0.1 mm. The experimental data have been taken from Ref. /18/. The value of ξ_0 = 1 corresponds to ω = 65 MeV.

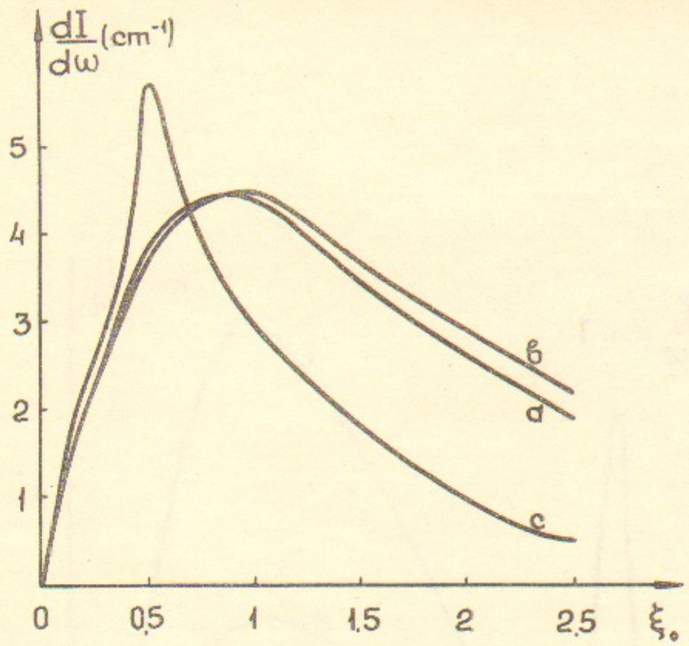

Fig.1

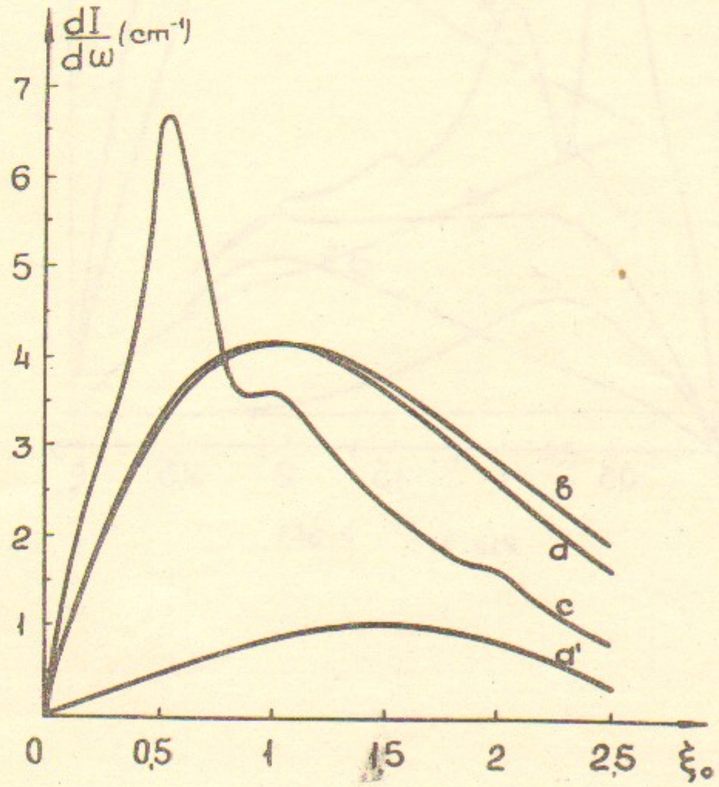

Fig.2

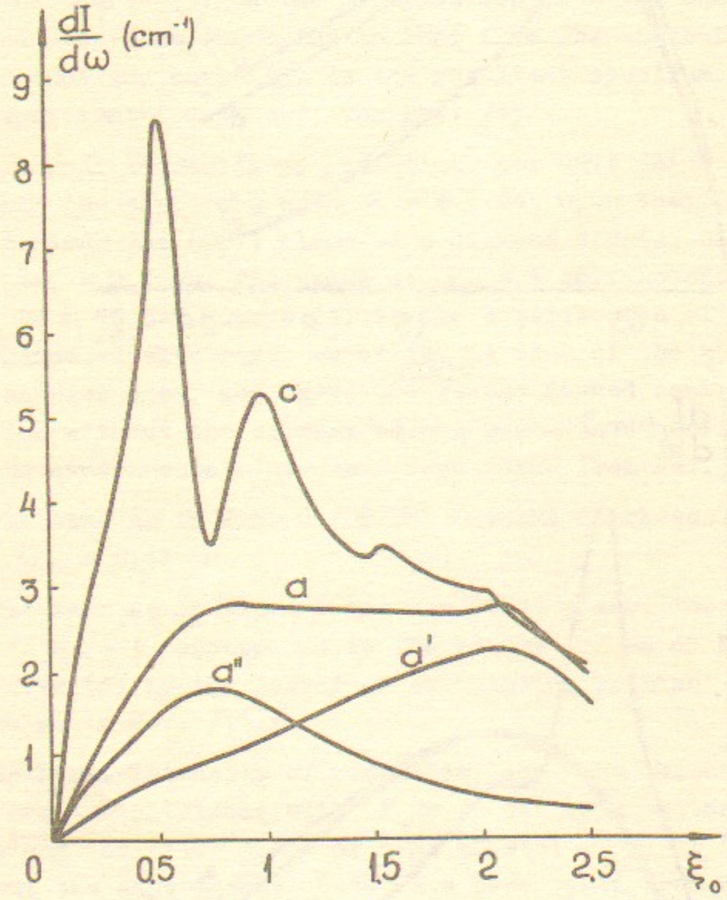
dI/dω (cm⁻¹)
9
8
7
6
5
4
3
2
1
c
a
a''
a'
0
0.5
1
1.5
2
2.5
ξ₀

Fig.3

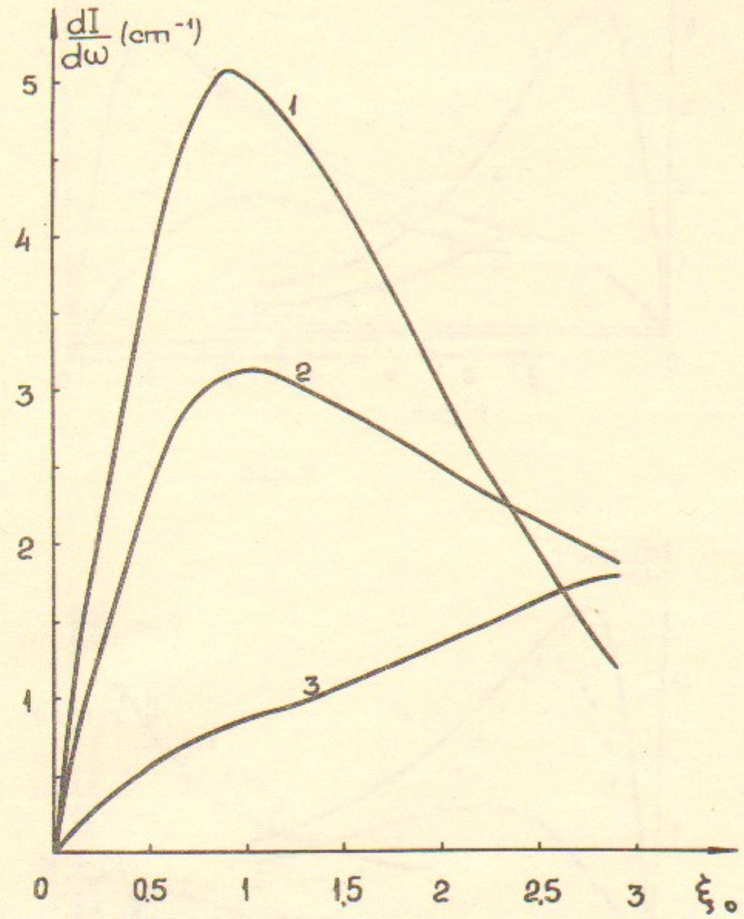
dI/dω (cm⁻¹)
5
4
3
2
1
1
2
3
0
0.5
1
1.5
2
2.5
3
ξ₀

Fig.4

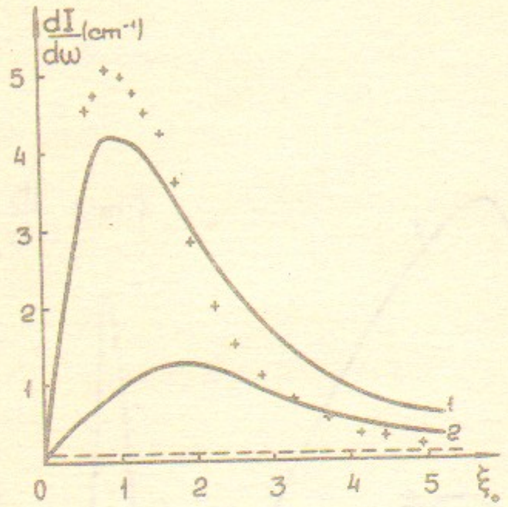

Fig.5

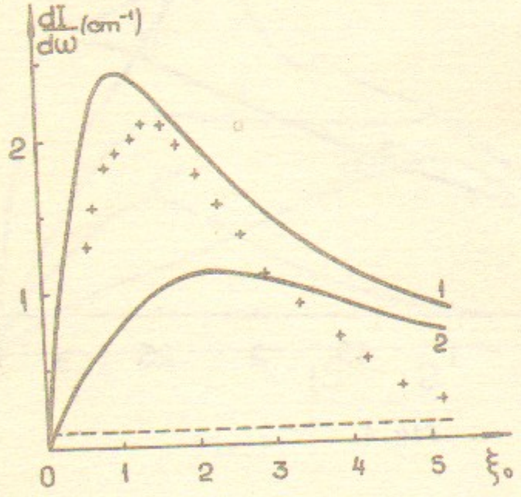

Fig.6

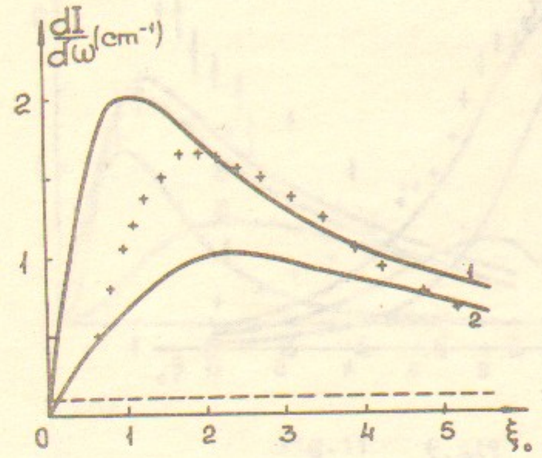

Fig.7

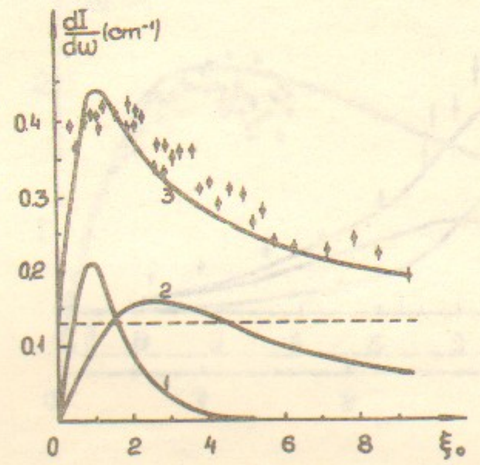

Fig.8

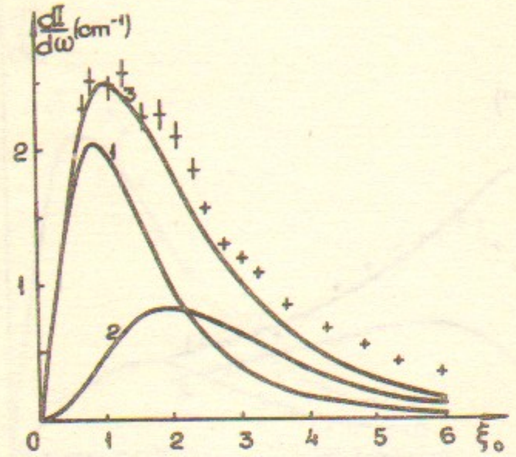

Fig.9

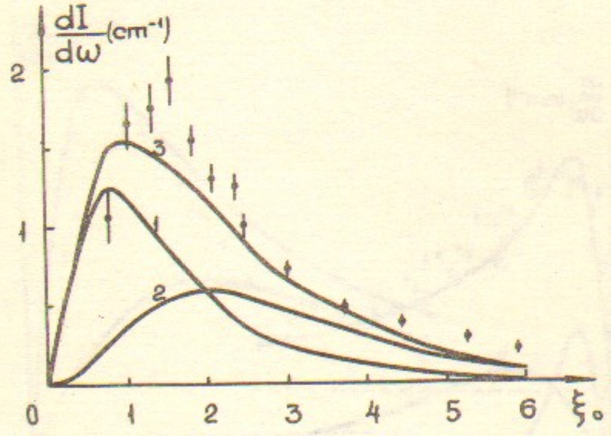

Fig.10

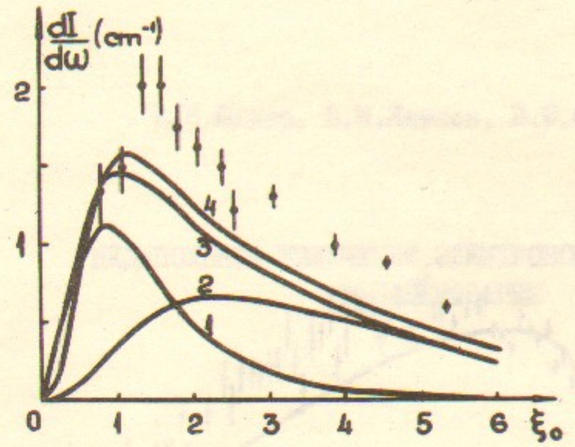

Fig.11

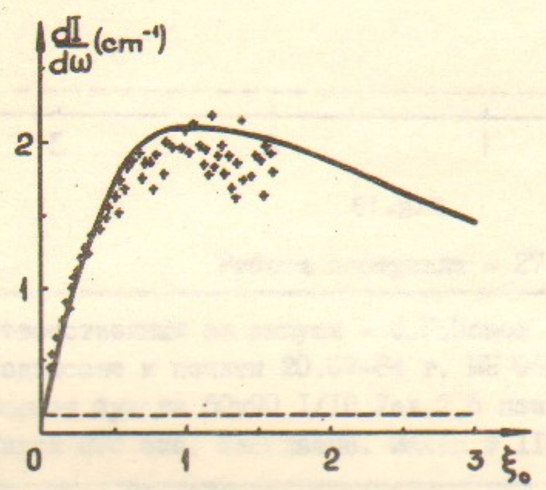

Fig.12

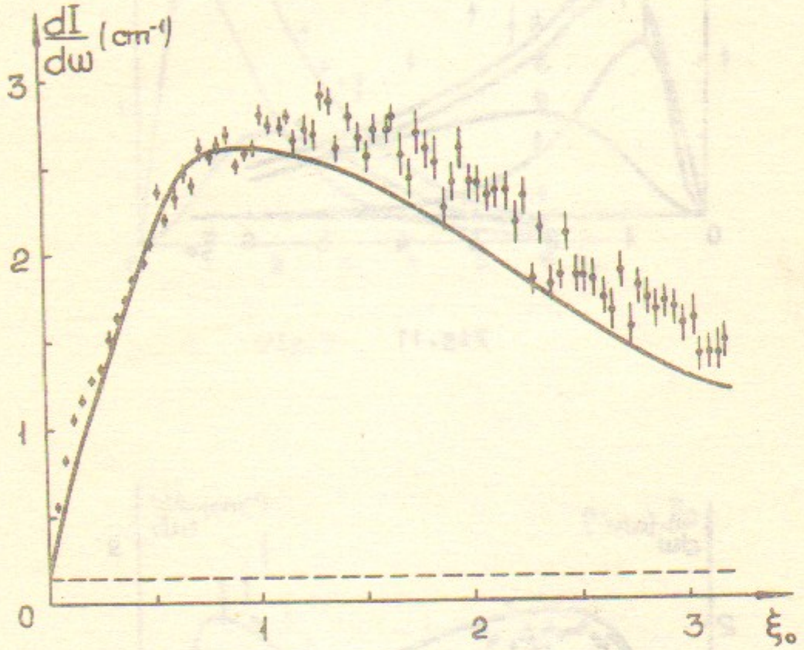

Fig.13

В.Н.Байер, В.М.Катков, В.М.Страховенко

НЕДИПОЛЬНОЕ ИЗЛУЧЕНИЕ ЭЛЕКТРОНОВ ПРИ ПЛОСКОСТНОМ КАНАЛИРОВАНИИ

Препринт
№ 84-116

Работа поступила - 27 февраля 1984 г.

Ответственный за выпуск - С.Г.Попов
Подписано к печати 20.07-84 г. МН 04463
Формат бумаги 60x90 1/16 Усл.2,5 печ.л., 2,0 учетно-изд.л.
Тираж 290 экз. Бесплатно. Заказ № 116.

Ротапринт ИЯФ СО АН СССР, г.Новосибирск, 90